Can the zircon origin be established from geochemical data alone? Insights from chlorite schists in the Ronda peridotites

¿Bastan los datos geoquímicos para establecer el origen del circón? Aportaciones de los esquistos cloríticos en las peridotitas de Ronda

José Julián Esteban, Julia Cuevas and José María Tubía

Departamento de Geodinámica, Facultad de Ciencia y Tecnología, Universidad del País Vasco (UPV/EHU), apartado 644, 48080 Bilbao jj.esteban@ehu.es; julia.cuevas@ehu.es; jm.tubia@ehu.es

ABSTRACT

This study deals with the scarce chlorite schists scattered through the Ronda peridotites (Betic Cordilleras, Spain) related to the intrusion of granite dykes. Chlorite schists field data and the petrography, geochemistry and geothermometry of the extracted zircon crystals, point to late magmatic melts for the zircon origin. Moreover, LA-ICP-MS analyses reveal that trace and rare earth elements alone could not be indicative for the magmatic or hydrothermal origin of zircon. Therefore, the combination of that information with zircon morphology, melt inclusions, geothermometry, and structural data, when possible, is crucial in the correct zircon origin identification.

Key-words: *Betic Cordillera, Ronda peridotites, chlorite schists, zircon, REE.*

RESUMEN

Este trabajo se centra en los escasos esquistos cloríticos, asociados a la intrusión de diques graníticos, que se encuentran en las peridotitas de Ronda (Cordilleras Béticas, España). A partir de los datos de campo de los esquistos y de la petrografía, geoquímica y geotermometría de circones extraídos, se concluye que su origen está ligado a fluidos magmáticos tardíos. Además, la información obtenida mediante LA-ICP-MS confirma que los elementos trazas y las tierras raras por sí solos no son determinantes acerca del origen magmático o hidrotermal del circón. Por tanto, la combinación de dicha información con la morfología de los circones, inclusiones de fundidos, geotermometría y el estudio estructural, en el caso de ser posible, es crucial para la correcta identificación del origen del circón.

Palabras claves: *Cordilleras Béticas, peridotitas de Ronda, esquistos cloríticos, circón, REE.*

Geogaceta, 68 (2020), 23-26
ISSN (versión impresa): 0213-683X
ISSN (Internet): 2173-6545

Fecha de recepción: 29/01/2020
Fecha de revisión: 23/04/2020
Fecha de aceptación: 29/05/2020

Introduction

Most publications about the Ronda peridotites (Betic Cordilleras, southern Spain) have focused in geochemical, petrological and structural topics but issues related to its serpentinization and rodingitization processes have passed almost unnoticed. The term rodingite (Bell *et al*., 1911) refers to Ca-enriched and SiO_2-undersatured metasomatic rocks rich in Ca-Al and Ca-Mg silicates, products of the metasomatism of silicate rocks in contact with or within serpentinized ultramafic rocks. These rocks are commonly wrapped by chlorite shells, which are referred to as blackwalls or chlorite schists (*e.g.,* Dubinska *et al*., 2004), formed from the alteration of the ultramafic rocks.

During decades zircon has been considered to be a rare or absent mineral in ultramafic rocks due to the low Zr content and Si activity of these rocks. However, zircon is being increasingly reported within mantle-derived xenoliths, mafic granulites, peridotites, pyroxenites, rodingites and blackwalls. This work reports a geochemical and petrographical study of zircon crystals from chlorite schists in the Ronda peridotites. These chlorite schists outstand by its high zircon content and have been described as blackwall zones formed, during the serpentinization of the ultramafic rocks, by interactions between the ultramafic rocks and granite dykes (Esteban *et al*., 2007). However, although the chlorite schist formation is linked to peridotite serpentinization, the origin of the zircon crystals is still unclear.

Geological setting

The Ronda peridotites are the largest orogenic lherzolites massifs in the world and correspond mainly to spinel and plagioclase peridotites with subordinate mafic layers (Obata, 1980). These massifs are tectonically sandwiched into the middle continental crust of the metamorphic Internal Zone of the Betic Cordilleras (Tubía, 1994).

The studied area is located in the south-western part of the Sierra Bermeja massif (Fig. 1), where the peridotites, displaying a dominant NNE foliation parallel to the mafic layering, are traversed by granite dykes (Cuevas *et al*., 2006). The peridotites are weakly to strongly serpentinized around the dykes. These dykes have great textural and mineralogical variations enhanced by the late formation of amphibole and other calcium-rich minerals during rodingitization events (Esteban *et al*., 2003). These dykes have been linked to a short-lived event of partial melting of the crustal rocks underlying the Ronda peridotites during their hot emplacement.

Metric-sized layers and pods of zircon-bearing chlorite schists, parallel to granite dykes and normal to the mafic layering, are present. Their structural relationship precludes an origin from older mafic layers and link the chlorite schists to the granite dyke intrusion (Esteban *et al*., 2007).

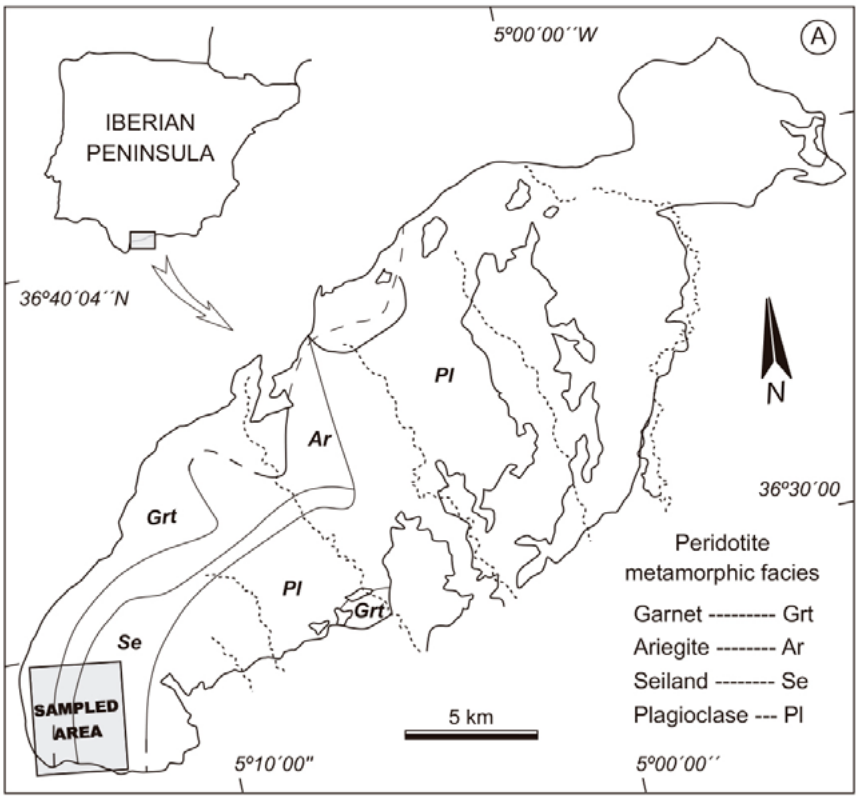

Fig. 1.- Geological location of the chlorite schists within the Ronda peridotites. Petrographic zonation from Obata (1980).
Fig. 1.- Localización geológica de los esquistos cloríticos en las peridotitas de Ronda. Zonación petrográfica según Obata (1980).

Chlorite schist zircon crystals

Petrographic features

Zircon crystals were separated by conventional mineral separation techniques from three chlorite schists samples. Crystals are idiomorphic and display sub-equant habits with a mean long axis ranging between 80 and 230 µm. Prismatic zircon crystals (*ca.* 200 µm long and 100 µm wide), while less common than idiomorphic, are also present. Back-scattered electron (BSE) images obtained by using a scanning electron microscope (JEOL 6400-JSM) reveal idiomorphic zircon crystals with dominant sector zoning and weak oscillatory zoning. No inherited cores were detected (Fig. 2A).

Zircon crystals often contain inclusions with ovoid, hourglass, droplet and irregular shapes (Fig. 2B). Their size ranges from a few to a few tens of micrometers. Tiny gas bubbles and primary decrepitation textures are also identified. These inclusions are frequently formed by two-contrasted glasses and include small idiomorphic white mica, apatite, quartz, feldspar, rutile, phlogopite and thorite (Fig. 2C). The qualitative EDX analyses yield mostly strong silicic and peraluminous ([SiO_2] > 70 %; ASI > 1) compositions. All these features are consistent with silicate melt inclusions (*e.g.,* Thomas *et al*., 2003).

Cathodoluminescence images of zircons from four granite dykes were also taken at the VSEGEI of Saint Petersburg (Russia), in order to show the microstructural differences between the zircon crystals from the dykes (Fig. 2D) and the chlorite schists (Fig. 2A). In contrast with the chlorite schist zircons, the granite ones have inherited oscillatory zoning cores and peripheral growth rims assessing multigrowth stages. Therefore, the lack of inherited cores of the chlorite schist zircon crystals indicates that they cannot be interpreted as xenocrysts dragged from the granite dykes.

Zircon trace and rare earth elements (REE) geochemistry

Trace and REE were analyzed by Laser Ablation ICP-MS at the University of the Basque Country (IBERCRON - SGIker). REE abundances were normalized to C1-chondrite of McDonough and Sun (1995). All chondrite patterns (Fig. 3A) are quite similar and are strongly depleted in light REE (LREE) content, display a very steep positive slope from La to Lu [$(Lu/La)_N$ > 5000], a large Ce positive anomaly (Ce*= 11 - 278, mean of 110) and a smaller negative Eu anomaly (Eu*= 0.24 - 0.35, mean of 0.31), suggesting a common origin for all the zircons. Measured Th/U ratios display an average value of 0.15 (Fig. 3B).

Zircon crystallization temperature was calculated according to the Ti-in-zircon content calibration of Watson *et al*. (2006). The activity of SiO_2 and TiO_2 was considered to be 1 due to the presence of quartz and rutile inclusions within zircon. The measured Ti concentration ranges from 3.21 to 5.32 ppm, with a mean value of 3.9 ppm. The application of the Watson *et al*. (2006) geothermometer yields mean temperatures from 672 ± 6 to 658 ± 4 ºC for the analyzed samples. A pressure correction for the Ti-in-zircon thermometer has to be also taken into account, as such temperature values are estimated for a pressure of 10 kb but temperature drops 50 ºC at pressure conditions of 1 kb (Watson *et al*., 2006). A pressure of 4.2 kb proposed for dyke intrusion by Tubía *et al*. (1997) was considered. Therefore, assuming a linear temperature/pressure dependence in the Ti-in zircon geothermometer, the temperature would be *ca*. 20 ºC below the calculated

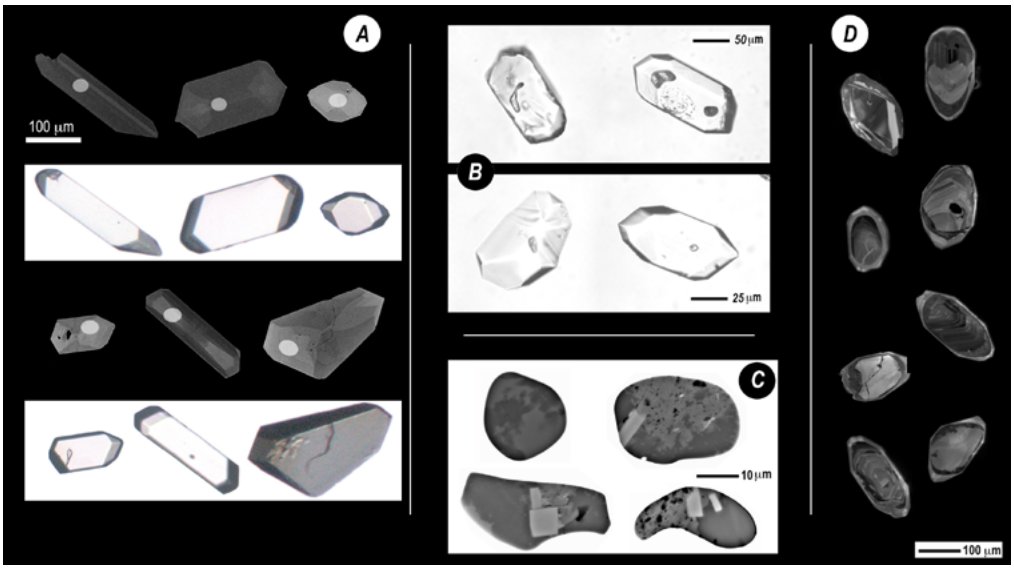

Fig. 2.- A) Photomicrographs and backscattered electron images of chlorite schist zircon crystals. B) Photomicrographs of melt inclusions with hourglass, droplet-shaped and bubbles bearing inclusions. C) Backscattered electron images of melt inclusions. Note two differentiated colored glasses and light color idiomorphic crystals of white mica. D) Cathodoluminescence images of granite dyke zircon crystals that show clear core and rim microstructure.

Fig. 2.- A) Microfotografías e imágenes de electrones retrodispersados de los circones de los esquistos cloríticos. B) Microfotografías de inclusiones de fundidos con geometrías en gota, en reloj de arena y con burbujas. C) Imágenes de electrones retrodispersados de inclusiones de fundidos. Véase la diferencia de color entre los dos vidrios y los cristales idiomorfos de mica blanca. D) Imágenes de catodoluminiscencia de circones de los diques graníticos, donde se observa la presencia núcleos y bordes.

values. Therefore a range between 630 and 655 ºC can be considered as a good approximation to the crystallization temperature of the analyzed zircon. These temperatures are significantly higher that those (289-322 ºC) reported previously for the chlorite schists formation (Esteban *et al*., 2007), but are consistent with the thermal conditions proposed for the emplacement of the granite dykes in the Ronda peridotites (Cuevas *et al*., 2006).

Discussion: Zircon origin

According to the literature, magmatic and hydrothermal zircon crystals can display distinct REE and trace elements patterns that can be used as discrimination criteria for their origin. While hydrothermal zircons commonly display REE distribution patterns characterized by flat or slight slopes from La to Sm and steep ones from Sm to Lu with and small Ce anomalies, the magmatic ones display steeper slopes from La to Lu and large Ce anomalies. However, some hydrothermal zircons can show "magmatic-like" REE patterns. In fact, the REE distribution in zircon, apart from its origin, can be a function of the crystallization sequence of accessory minerals (apatite, xenotime, monazite, allanite, ilmenite), the temporal changes in the magma composition, complex substitution mechanisms or even accidental sampling of REE-bearing micro-inclusion, among others (*e.g.* Chapman *et al.*, 2016). In spite of displaying clear magmatic affinity, the geochemistry of the studied zircon crystals has been tested against zircon compositions from some hydrothermal environments with either "hydrothermal-like" (Fig. 3A) or "magmatic-like" (Fig. 3B) REE patterns (Hoskin, 2005; Pettke *et al*., 2005; Guo *et al*., 2011; Fukuyama *et al*., 2014; Zhu *et al*., 2016; Hu *et al*., 2017). The analyzed zircons can be also classified as hydrothermal zircons with "magmatic-like" REE patterns (Fig. 3A). This ambiguity states that the REE patterns alone are not indicative of their origin.

In the U *vs*. Th or U/Ce *vs*. Th bilogarithmic diagrams (Castiñeiras *et al*., 2011), the studied samples plot in the field of magmatic rocks (Figs. 3C and D). The Ta/Nb and HfO_2/Y_2O_3 ratios are commonly used to discriminate the nature for early magmatic zircons from late magmatic or hydrothermal (Pettke *et al*., 2005), as early magmatic zircons do show lower Ta/Nb and HfO_2/Y_2O_3 ratios (usually < 1). The mean value (≈ 1) of the Ta/Nb in the analyzed zircon crystals prevents its use as a possible discrimination parameter. In contrast with the high HfO_2/Y_2O_3 values (from 1.45 to 7.86) that are consistent with a late magmatic origin of the zircon. Bilogaritmic plots of Hoskin (2005) also agree with zircons being of magmatic origin (Figs. 3E and F).

Three different origins could be considered for these zircons: early magmatic, late magmatic and hydrothermal. The finding of melt inclusions and the high Ti-in-zircon crystallization temperatures discard the hydrothermal origin. Alternatively, an early magmatic origin directly coupled with the intrusion of the granite dykes could be considered from the structural relationships between the dykes and the chlorite schists. However, the huge microstructural contrast between the zircons extracted from the granite dykes and the chlorite schists also rules out the interpretation or zircons being xenocrysts dragged from the neighbour granite dykes. An additional option arises when different types of data are combined. Taken together, the "magmatic-like" REE patterns, crystallization temperatures, melt inclusions and lack of fluid inclusions point to late (highly-differentiated) melts sourced from the dykes. In this regard, the geochemistry of zircon crystals from the Ronda chlorite schists is consistent with previous results (Pettke *et al*., 2005) in the Mole Granite, showing that high temperature hydrothermal zircon crystals have similar REE patterns than late magmatic ones.

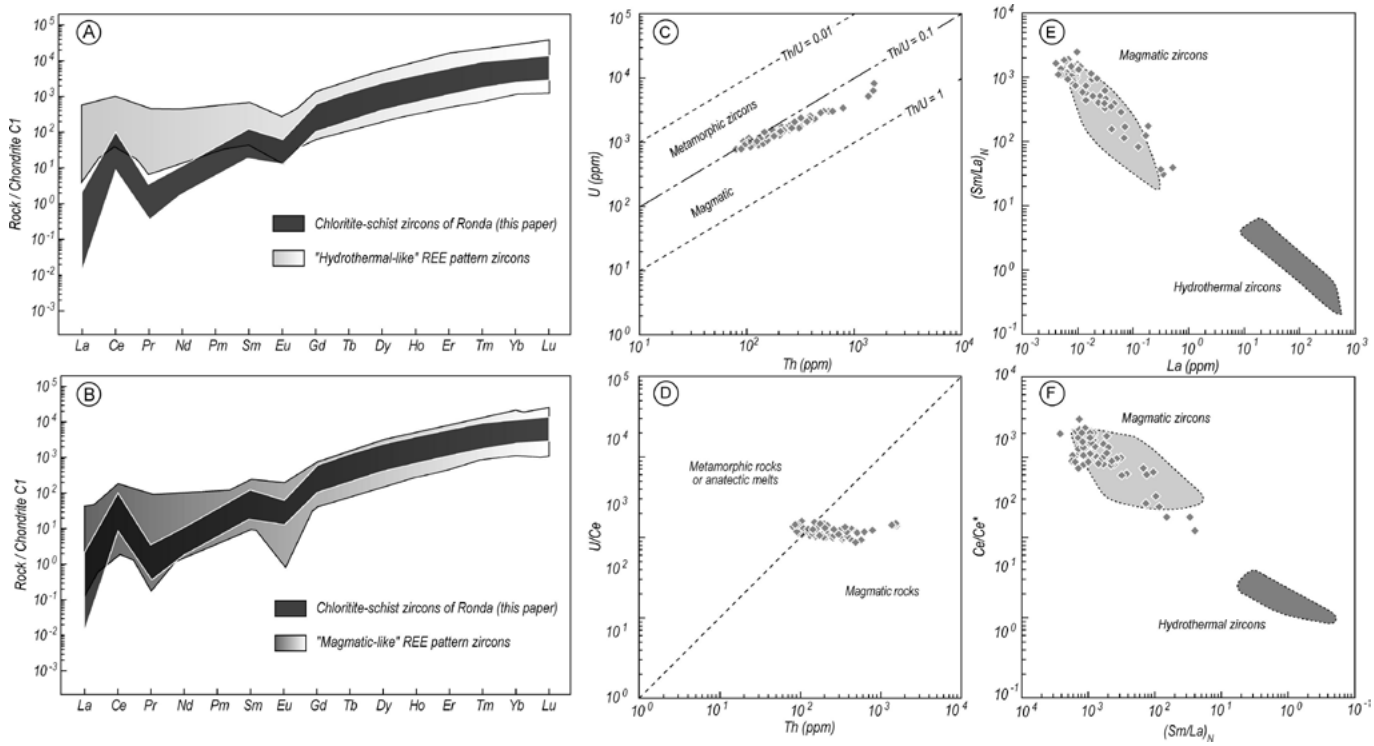

Fig. 3.- Comparative normalized REE diagram (C1 Chondrite; McDonough and Sun, 1995) of chlorite schist zircons to "hydrothermal" (A) and "magmatic-like" (B) hydrothermal zircon crystals. U *vs*. Th (C), U/Ce *vs*. Th (D), (Sm/La)N *vs*. La (E) and Ce/Ce* *vs*. (Sm/La)N (F) discrimination diagrams for metamorphic, hydrothermal and magmatic zircon crystals.

Fig. 3.- Diagramas normalizados de REE de circones de los esquistos cloríticos (Chondrito C1; McDonough y Sun, 1995) comparados con circones hidrotermales con patrones de REE de afinidad hidrotermal (A) y magmática (B). Diagramas U vs. Th (C), U/Ce vs. Th (D), (Sm/La)N vs. La (E) y Ce/Ce* vs. (Sm/La)N (F) de discriminación entre circones metamórficos, hidrotermales y magmáticos.

Conclusions

(1) The REE patterns by themselves are not diagnostic tools for deciphering the magmatic or hydrothermal origin of zircon, as "magmatic-like" REE patterns can be found in both magmatic and hydrothermal zircons.

(2) The presence of silicate melt-inclusions confirms the magmatic nature of chlorite schist zircons.

(3) Ti-in-zircon geothermometry yields temperatures of 630-655 ºC for zircon crystallization.

(4) A late magmatic melt is proposed for the zircon origin.

Acknowledgements

This work has been supported by grants GIU17/033 of the *"Grupos de Investigación"* of the University of the Basque Country and CGL2017-82976-P (Ministerio de Economía, Industria y Competitividad/AEI/FEDER). Gabriel Gutiérrez-Alonso and an anonymous reviewer are thanked for their time in the careful reviews of the manuscript.

References

Bell, J.M., Clarke, E. de C. and Marshall, P. (1911). *New Zealand Geological Survey Bulletin* 12, 71.

Castiñeiras, P., Navidad, M., Casas, J.M., Liesa, M. and Carreras, J. (2011). *The Journal of Geology* 119, 521-534.

Chapman, J.B., Gehrels, G.E., Ducea, M.N., Giesler, N. and Pullen, A. (2016). *Chemical Geology* 439, 59-70.

Cuevas, J., Esteban, J.J. and Tubía, J.M. (2006). *Journal of the Geological Society* 163, 631-640.

Dubinska, E., Bylina, P., Kozlowski, A., Dörr, W., Nejbert, K., Schastok, J. and Kulicki, C. (2004). *Chemical Geology* 203, 183-203.

Esteban, J.J., Cuevas, J., Tubía, J.M. and Yusta, I. (2003). *Canadian Mineralogist* 41, 161-170.

Esteban. J.J., Cuevas, J., Tubía, J.M., Liati, A., Seward, D. and Gebauer, D. (2007). *Lithos* 99, 121-135.

Fukuyama, M., Ogasawara, M., Dunkley, D.J., Wang, K.L., Lee, D.C., Hokada, T., Maki, K., Hirata, T. and Kon, Y. (2014). *The Island Arc* 23, 281-298.

Guo, H., Du, Y., Yang, J. and Guo, L. (2011). *Science China-Earth Sciences* 54, 1675-1685.

Hoskin, P.W. (2005). *Geochimica et Cosmochimica Acta* 69, 637-648.

Hu, C.N., Santosh, M., Yang, Q.Y., Kim, S.W., Nakagawa, M. and Maruyama, S. (2017). *Lithos* 274-275, 349-362.

McDonough, W.F. and Sun, S.-s. (1995). *Chemical Geology* 120, 223-253.

Obata, M. (1980). *Journal of Petrology* 21, 533-572.

Pettke, T., Audétat, A., Schaltegger, U. and Heinrich, C.A. (2005). *Chemical Geology* 220, 191-213.

Thomas, J.B., Bodnar, R.J., Shimizu, N. and Chesner, C.A. (2003). *Reviews in Mineralogy & Geochemistry* 53, 63-87.

Tubía, J.M. (1994). *Tectonophysics* 283, 381-398.

Tubía, J.M., Cuevas, J. and Gil Ibarguchi, J.I. (1997). *Tectonophysics* 279, 227-252.

Watson, D.A., Wark, D.A. and Thomas, J.B. (2006). *Contributions to Mineralogy and Petrology* 151, 413-433.

Zhu, J., Peng, S. and Peng, L. (2016). *Resource Geology* 66, 227-239.